Molecular Vision 2025; 31:142-157 <http://www.molvis.org/molvis/v31/142>
Received 12 September 2023 | Accepted 27 March 2025 | Published 29 March 2025

Multikinase inhibition-mediated proliferative vitreoretinopathy therapy by nanoparticles in rabbits

Elif Arslan,[1,2] Faruk Ozturk,[1] Burcu Uner,[3,4,5] Serkan Tureli,[6] Sevda Fatma Muftuoglu,[6] Cetin Tas[3]

[1]Department of Ophthalmology, Hacettepe University School of Medicine, Ankara, Turkey; [2]Department of Ophthalmology, Ulucanlar Eye Education and Research Hospital, Ankara, Turkey; [3]Department of Pharmaceutical Technology, Yeditepe University, Faculty of Pharmacy, Istanbul, Turkey; [4]Department of Pharmaceutical and Administrative Sciences, University of Health Science and Pharmacy in St. Louis, St. Louis, MO; [5]Department of Pharmaceutical Technology, Istanbul Kent University, Faculty of Pharmacy, Istanbul, Turkey; [6]Department of Histology and Embryology, Hacettepe University School of Medicine, Ankara, Turkey

Purpose: To investigate the efficacy of nanoparticles in treating proliferative vitreoretinopathy (PVR) through clinical observation, histology, and immunohistochemistry, despite unsatisfactory surgical outcomes and failed therapies for the current PVR treatment

Design: Twelve rabbits were divided into control and nintedanib (NTB) groups. The rabbits underwent weekly ophthalmologic examinations over a period of four weeks.

Methods: At the end of the fourth week, the rabbits' eyes were removed for histological and immunohistochemical evaluation. Three additional rabbits outside the PVR model were administered a 0.5% NTB-loaded liposomal formulation in one eye. The drug concentrations in the vitreous samples were determined using high-pressure liquid chromatography on days 1, 7, 14, and 35.

Results: The PVR stages were low in the NTB group, and there was no significant difference between the NTB and control groups ($p = 0.108$). However, it is worth noting that the group treated with NTB had significantly fewer epiretinal membrane formations during the histological evaluation. In addition, the corrected fluorescence intensity measurement of the subjects for collagen-1 in the NTB group was significantly lower than that in the control group ($p = 0.004$). Most importantly, no significant adverse effects were observed.

Conclusions: Our study has provided preclinical support for a liposomal formulation containing NTB that, with single-dose administration, has the potential to be effective in vivo in preventing the development of PVR and its correlated pathologies without causing any significant side effects.

Proliferative vitreoretinopathy (PVR) poses a grave threat as a complication of ocular trauma and is frequently the primary reason for unsuccessful rhegmatogenous retinal detachment (RRD) surgery [1]. The process of healing wounds through PVR is distinct because it involves the growth and contraction of cell membranes on the vitreous cavity and retinal surface. The contraction of these membranes may result in macular shrinkage (macular pucker), new retinal tears, recurrent retinal detachments, and ocular hypotonia [1-4]. The incidence of PVR in RRD cases is considered to be 5%–10% [5]. It is the main cause of eventual surgical failure, a condition that has largely remained despite advances in vitreoretinal surgery techniques and equipment [5].

No known medication has been proven to effectively treat or prevent PVR. The mainstay of treatment for PVR is surgical intervention [4,6]. Numerous studies have been conducted to comprehend the pathophysiology of vitreoretinal conditions and to identify the risk factors associated with PVR. These studies aimed to provide guidance for the development of molecular-targeted therapies. The drugs that have been investigated for PVR target one or more of the associated pathologies, including anti-inflammatory, antiproliferative, antineoplastic, anti-growth factor, and antioxidant agents. Although many agents have had good results in preclinical studies, most of these therapies have failed in human clinical trials [7,8]. Therefore, more studies targeting specific pathways are needed to achieve better visual outcomes in the prophylaxis and treatment of PVR.

In 2014, nintedanib (NTB) became the first multikinase inhibitor approved by the FDA for the treatment of idiopathic pulmonary fibrosis (IPF). This medication inhibits small molecules known as kinases by targeting the receptors for platelet-derived growth factor in both alpha and beta forms, as well as the receptors for fibroblast growth factor in types 1–3, and vascular endothelial growth factor (VEGF) in types 1–3 [9]. It acts as a competitive inhibitor by occupying the adenosine triphosphate (ATP)-binding sites of the

Correspondence to: Elif Arslan, Department of Ophthalmology, Ulucanlar Eye Education and Research Hospital, Ulucanlar Street, 06250, Ankara, Turkey; Phone: +905388388916; email: elif_guler@hacettepe.edu.tr

target kinases and preventing their activation. Cell growth and programmed cell death are impeded by this substance through the blocking of protein kinase signaling pathways in three distinct types of cells—endothelial cells, pericytes, and smooth muscle cells—which play crucial roles in the formation of new blood vessels [10].

Liposomes, which are biocompatible, biodegradable, non-immunological, low-toxic, and double-layered, are delivery systems with spherical vesicular encapsulating surfaces consisting in part of amphiphilic phospholipid building blocks [11,12]. They can carry both hydrophilic and hydrophobic drugs and, by controlled release, increase accumulation in the target region [13]. The purpose of this project was to evaluate the effect of intravitreal liposomal delivery of the multikinase inhibitor NTB on PVR formation. The study included investigations of NTB's blocking mechanisms that may control alternative pathways toward PVR formation, using cell culture, clinical evaluation, and histological and immunohistochemical studies. In this way, we investigated and compared the effectiveness of three different treatment approaches for the PVR model. These approaches included using a bulk solution of NTB, not using any treatment with NTB, and using NTB-loaded liposomes. Through in-depth analysis and experimentation, we were able to determine a treatment method that could be considered optimal for the PVR model.

METHODS

Materials: NTB was purchased from MedChemExpress (Monmouth Junction, NJ). Egg-phosphatidylcholine (PhCH), cholesterol (CHO), and potassium phosphate were obtained from Sigma-Aldrich (Munich, Germany). Xylene, hematoxylin, eosin, and paraffin were purchased from Fisher Scientific (Hunting Hill, NJ). Collagen-1 monoclonal antibody stain (MA1–26771, NJ), crystal violet, secondary antibody Alexa Fluor 488 (A-11001, NJ), granulocyte-colony stimulating factor (G-CSF; G-CSF Human Instant ELISA™ Kit), VEGF (BMS277–2TEN, Human VEGF Quantikine ELISA Kit), nuclear factor kappa (Nf-κB; p65, (Total) Human InstantOne™ ELISA Kit), tumor necrosis factor alpha (TNF-α; A35601, TNF alpha Human ProQuantum Immunoassay Kit), and Triton X (151500) were provided from Thermo Fisher, Atlanta, GA. All chemicals used in the analysis had a high-pressure liquid chromatography (HPLC) grade (higher than 99% purity). Double-distilled water was used in all the experimental processes.

Preparation of NTB lyposomes: Liposomes confining NTB (0.05% w/w) were fabricated using dehydration–rehydration and freeze–thaw methods [14]. PhoCH and NTB (9.3 mM) were dissolved in MeOH:chloroform (2:1, v/v). The solution in the flask was vaporized in a rotary evaporator (Heidolph, Germany) by decreasing the pressure gradually. After completing the evaporation process, 10 mL of phosphate buffer saline (PBS; 0.1 mmol/L, pH 7.4) was added to the flask. Subsequently, the mixture was sonicated in an ultrasonic bath (Isolab, Germany) for 10 min (Table 1). Then, NTB-liposome formulation (NTB-LIP) was collected in an Eppendorf tube (20 ml) before filtering with 0.22 µm polycarbonate filter (Millipore Co., Billerica, MA) under UV light in a laminar-flow cabinet (Biobase). Subsequently, the liposome formulations underwent a freeze–thaw process for varying numbers of cycles (3, 5, and 10). Each cycle involved freezing the samples for 3 min at a liquid nitrogen temperature (−196 °C), followed by thawing for 3 min in a 40 °C water bath. After this process was finished, formulations were stored at −20 °C for 24 h. Thereafter, the frozen formulation was thawed at 25 °C ± 0.5 °C and was promptly vortexed for 10 min and then kept at +4 °C.

Characterization of the NTB liposomes: Liposomes were characterized by a dynamic light scattering (DLS) device (Zetasizer Nano ZS, Malvern Instruments, UK). NTB-LIP's particles and potential were collected by diluting the solution in water (1:20 v/v). The encapsulation efficiency (encapsulation efficiency) was calculated by performing HPLC analysis. The NTB-LIP solution (100 µl) was diluted with 1 ml MeOH and measured to facilitate HPLC. The equation is shown below (Equation 1) [15].

Encapsulation efficiency (%) =Total NTB in liposis / Total NTB weight × 100

Vitreous samples and quantitative analysis for investigating NTB release and availability: Following the injection of

Table 1. Components of NTB-Liposome formulation.

Contents	F1 (mM)	F2 (mM)	F3 (mM)
PhoCH	50	80	100
NTB	9.3	9.3	9.3
CHO	20 mM	20 mM	20 mM

CHO: Cholesterol; NTB: Nintedanib; PhoCH: Egg-Phosphotidylcholine

0.1 ml of either NTB-PBS (9.3 mM contains PBS injectable solution-control group) or NTB-LIP under general anesthesia in one eye of three rabbits without any PVR application, vitreous samples were taken on days 1, 7, 14, and 35. Before the samples were analyzed via HPLC (Agilent 1100, NJ), they were kept at +4 °C. After sampling, the subjects were euthanized, and their eyes were enucleated and kept in formaldehyde solution for histological examination of the effects of the drug on the normal retina.

Prior to analysis, the samples were subjected to extraction. Briefly, 2 ml of water was added directly to the supernatant containing the analytes in microwave-safe closed vessels. The mixture was then stirred at 60 °C for 10 min, with the addition of 10 ml of acetonitrile. After cooling, the vessels were opened, and the extracts were centrifuged at 2146 ×g for 15 min to separate the organic and aqueous phases. The organic phase was collected, concentrated, and dried under a nitrogen stream at 30 °C. The resulting dry extract was redissolved in 200 µL of mobile phase (2% acetonitrile and 98% 0.02 M phosphate buffer, pH 6.8), theoretically achieving an eightfold concentration increase compared to the original vitreous humor sample. The entire sample preparation process using PBS took approximately 20 min. Finally, a 15 µl aliquot of the prepared sample was injected into the chromatograph.

For reverse-phase HPLC analysis, an Agilent Zorbax Eclipse XDB-C18 column (250 × 3.0 mm, length over internal diameter, 5 µm particle size, Agilent Technologies Inc., Seattle, WA) was used. In the mobile phase, 20 mmol potassium phosphate buffer (pH 3.0) was mixed with 7 mmol acetonitrile (7:3). A flow rate of 0.6 ml/min was employed for the mobile-phase flow using the isocratic method at 35 °C. UV absorbance detection at 390 nm detected NTB's wavelength [16]. The total run time was 14 min, with a sample injection volume of 10 µl. Chromatograms were processed using Agilent Chemstation software (Agilent Technologies, Inc., CA).

Scanning electron microscope analysis: The liposome formulations' surface structures were evaluated using a scanning electron microscope (SEM; Zeiss EVO 40, Carl Zeiss). The device was operated at 100 kW. The lyophilized samples were coated using an Au coater (Leica EM ACE600).

Reverse transcription-polymerase chain reaction and enzyme-linked immunosorbent assay analysis: Seeding of human retina pigment epithelium (RPE) cell line ARPE-19 cells (ATCC® CRL-2302, Manassas, VA) was conducted in the upper chamber of 24-well Transwell plates (Corning, Inc., Corning, NY) using 100 µl DMEM/F12 media containing 0.5% fetal bovine serum (FBS). The lower compartment was forcefully filled with 600 µl DMEM/F12 media containing 10% FBS. The cells were subjected to different treatments for 8 h: NTB-PBS (9.3 mM), NTB-LIP (9.3 mM), only PBS (positive control), and 0.1% Triton-X-PBS (negative control). Thereafter, the migrated cells were fixed with 4% phosphoribosylformylglycinamidine (PFA) and stained with 0.1% crystal violet for 30 min [17]. Total RNA was isolated using the RNA extractor kit (AM9775, Thermo Fisher) and subsequently treated with RNase-free DNase I (AM7006, Thermo Fisher) so as not to contaminate DNA before proceeding with reverse transcription-polymerase chain reaction (RT-PCR). The RNA was then incubated with reverse transcriptase, deoxynucleoside triphosphates (0.2 mM), and an RT-1 primer (CCCTAGGAGGAC) for 1 h at 42 °C. Following cDNA synthesis, PCR components were added to the reaction mixture, including primers specific for Nf-kb (p65), VEGF-A, and TNF-α (all from Thermo Fisher). The mixtures underwent amplification through 50 PCR cycles with the following parameters: 95 °C for 90 s (denaturation), 60 °C for 90 s (annealing), and 72 °C for 180 s (extension). Images were taken under a fluorescent microscope (Olympus Corporation, Tokyo, Japan), and migrating cells were counted using FlowJo 7.6 software.

Enzyme-linked immunosorbent assay (ELISA) studies were conducted to determine the VEGF, TNF-α, and Nf-κB biomarkers using the corresponding kits and the plate reader (ThermoScientific, Multiskan GO, Atlanta, GA). Initially, the spectrophotometric analyses of all of the markers were performed at both the specific wavelengths (450–530 nm) and concentration intervals (31.25 pg/ml-1000 ng/ml) designated by the kits' protocols [18-21]. Before the start of the analysis, the cells were supplemented with 0.1% Triton X (except in the positive control group) for 5 min, creating a simulated PVR model. Then formulations were added to the cells (except in the positive and negative control groups) and incubated for 12 and 24 h [22,23].

Western blot assessment:

Buffer solution preparation—The mixture samples (stored in aliquots at 20 °C)/marker proteins at a 1:1 ratio were incubated with concentrated buffer (17,654; Sigma-Aldrich, St. Louis, MO) for 2 min at 100 °C. The samples were subjected to a centrifuge (20 min, 5000 G) to remove undissolved particles. A 10% (w/v) ammonium persulfate (APS) solution was added to the protein mixture (1.0 g of APS to 10.0 ml of ultrapure water).

Gel preparation phase (SDS–PAGE)—Different ratio solutions were combined while preparing the SDS–PAGE. The resolver solution had two different components (acrylamide and bisacrylamide; 06,867; Sigma-Aldrich, St.

Louis, MO), and the stacking solution also had two different members (separation gel 3× concentration and separation gel 5× concentration; 14,946, 19,505; Sigma-Aldrich) [24].

Running buffer—80 µl of the sample was mixed with 10 µl of 3,3′,5,5′-tetramethylbenzidine (prepared by dissolving 1% dimethyl sulfoxide) buffer. The 10 µl mixture was injected into the gaps. The electrophoresis experiment involved loading 125 ml of the sample inside the chamber and 375 ml of the buffer solution outside. Following the addition of the buffer, the electrophoretic migration of the sample was continuously monitored for 1 h at a voltage of 120 V. At the end of this period, the samples reached the finish line. The gel was removed from between the glasses and placed in a staining solution. It was kept for 24 h [25].

Viability assay: The trypsinized RPE cells were counted after transferring 96-well. 5,000 cells/100 µl were seeded into each well of the cell culture plates. The cells were kept in the incubator for one day so that they would adhere to the base of the plates. After this interval, the medium on the cells was aspirated. The formulations were prepared at the required concentrations in the media used for cells, containing 4.5 mM, 9.3 mM, and 18 Mm concentrations of NTB-PBS, NTB-LIP, medium (positive control group), and Triton X (negative control group) applied to the cells (medium was used as the control group). The formulations were incubated for 24 h after application to the cells (5% CO_2 at 37 °C). After this period, the procedures were continued according to the methyl thiazole tetrazolium bromide (MTT) method, which was the viability determination method used.

After the incubation period (5% CO_2 at 37 °C), 25 µl of the MTT solution (5 mg/ml in isotonic phosphate buffer) was applied to the wells. 80 µl of sodium dodecyl sulfate (SDS) solution (23%, pH 4.7) dissolved in 45% dimethyl formamide were added to all of the wells after 4 h of incubation, and the incubator was left running overnight [26]. At the end of this period, the plates were removed, and the absorbances of the solutions in the wells were read at 570 nm in a microplate reader (ThermoScientific, Multiskan GO).

Scratch assay: ARPE-19 cells were seeded at a density of 1×10^5 cells/well in six-well plates to examine cell migration. Using a 20 L pipette tip, a wound was generated by scraping an RPE monolayer, after which the cells were subjected, and the photos were taken using a light microscope (Leica DM750 HD Digital Microscope, Feasterville, PA) both at 0 and 24 h after scratch. FlowJo 7.6 software was used to analyze the percentage of RPE migration. At least three fields (magnification 10) per treatment were measured in each of the three separate experiments.

To examine the cell polarity, ARPE-19 cells were seeded on 12-well glass coverslip-coated trays for analysis. The scratched cells were subjected to a 24 h treatment with various chemicals. The cells were then fixed in 4% PFA for 15 min and treated with 9.3 mM NTB-PBS and NTB-LIP (additionally the control group was included in the study by

applying only media) overnight at 4 °C, followed by 1 h of incubation with fluorescein isothiocyanate (FITC)-conjugated secondary antibodies [27,28]. After washing, the coverslips were counterstained with Alexa Fluor 488 and observed using a confocal microscope (Leica Stellaris Confocal, Feasterville, PA).

Animals and experiment design: All animal procedures in this study complied with the animal care guidelines published by the Institute for Laboratory Animal Research. This study was approved by the Hacettepe University Animal Experiments Local Ethics Committee (Approval No. 2020/54) and the Yeditepe University Animal Experiments Local Ethics Committee (Approval No. 2021–868). The project was supported by the Hacettepe University Scientific Research Projects Coordination Unit (project code: THD-2021–19176).

Twelve white New Zealand rabbits of both sexes weighing approximately 2 kg were used to induce PVR formation. The rabbits were randomly divided into two groups (six rabbits per group) as follows: the control group (numbered C1–C6) and the NTB group (numbered N1–N6). After a 1-week acclimatization period, 35 mg/kg ketamine (Keta-control 10%, Doga Pharmaceuticals, Turkey) and 5mg/kg xylazine (Basilazine 2%, Bavet, Turkey) were administered intramuscularly to provide general anesthesia. Pupillary dilation was achieved by instilled tropicamide (Tropamide 0.5%, Bilim Pharmaceuticals, Turkey) into one randomly determined eye of each of the 12 rabbits, and an application was made to one eye of each subject. All experimental applications (needle injury+dispase injection) were made to only one dilated eye of rabbits in this section of the study.

After local anesthesia was provided with proparacaine (Alcaine 0.5%, Alcon, Belgium), fundus examination was performed on all subjects with an indirect ophthalmoscope and a 20D lens, and it was confirmed that the fundi had anatomically normal structures. Then, the conjunctiva was cleaned with 5% povidone iodine, and a 23G needle was inserted approximately 5 mm behind the superior limbus at the 11 o'clock position. During the procedure, care was taken not to touch the lens or other surrounding tissues. Under an indirect ophthalmoscope, the needle was gently inserted into the vitreous cavity at a 45 ° angle, and the sharp tip touched the retina, causing vitreous hemorrhage and puncture injury, as in a previous study [30] (Figure 1). At this time, the needle

Table 2. Equations of dissolution rate parameters in pharmacokinetic perspective.

Parameter	Equation (Excel Formula Format)
Cmax, Maximum concentration in the vitreous part	=C0/(1-EXP(-ke*r))
Half-life (T1/2), Time that passed for spending the NTB's half of dose	=0.693/ke
Tmax, Time to attain maximum concentration for vitreous part	=LN(ka/ke)/(ka-ke)
MRT, mean residence time of the NTB substance molecules in the dosage form	=SUMPRODUCT(t_range, (100 - y_range))/SUM(100 - y_range)
DE, dissolution efficiency	=SUM(y_range)/(y100*t)*100

ka: absorption velocity consant, ke: elimination constant, n: number of sampling points, r: mean radius of eye, y: percentage of drug dissolved at time t, y_{100}: maximum percentage of drug dissolved over the time period 0−t

was slightly withdrawn, and 0.1 ml of vitreous aspiration was performed. Just above the damaged area, 0.05 U/0.1 ml dispase solution (Boehringer Mannheim) was injected by changing the injector part. Because the dose causing the formation of vitreous haze and cataract at an acceptable level in previous studies was determined to be 0.05–0.07 U, the application was made at this dose [31,32]. When the mid-vitreous was reached during the slow withdrawal of the needle, the injector part was changed, and the injection was made according to the group in which the subjects were randomly determined. 0.1 ml of 0.5% NTB was injected into the mid-vitreous of six randomly selected rabbits. 0.1 ml of PBS was injected into the mid-vitreous of the six other rabbits, which were assigned as the control group. Tobramycin (Tobrased 0.3%, Bilim Pharmaceuticals, Turkey) was instilled in all treated eyes immediately after the injections. The pharmacokinetic parameters of the formulations were calculated according to Table 2 [29]. At the end of week 4, the subjects were euthanized with high-dose ketamine and xylazine, and their eyes were enucleated. The enucleated eyes were fixed in formaldehyde solution for histological and immunohistochemical examinations.

Ophthalmologic examination: After the creation of the experimental model, the subjects underwent a weekly fundus examination under general anesthesia for four weeks, and the fundus images were recorded with a smartphone camera. The fundus findings were graded according to the Fastenberg scale [33]. At the end of week 4, an anterior segment examination was performed with a portable slit lamp (SL-15, Kowa, Japan). The subjects were examined for corneal edema, uveitis, and lens opacity.

Histopathology and immunohistochemistry: The tissues were fixed in 4% phenol-containing formaldehyde with 10% phosphate buffer after the rabbit eyes were enucleated to soften the lens. After fixation, the tissues were processed using an automatic benchtop tissue processor (Leica TP1020, Leica Microsystems, Germany) to prepare them for embedding. For histological analysis and bright-field microscopy (Leica DM6000 B, Leica Microsystems, Germany), formalin-fixed paraffin-embedded tissue sections were stained with hematoxylin eosin and trichrome stain (BO 04–001802, Bio-Optica, Italy).

Indirect immunofluorescence was performed using anticollagen-1 monoclonal antibody (MA1–26771, Thermo Fisher Scientific) and secondary antibody Alexa Flour 488 (A-11001, Thermo Fisher Scientific). DAPI (FluorLast™ with DAPI, BioVision) was used for nuclear staining. The stained sections were examined under a fluorescent microscope (Leica DM6000 B, Leica Microsystems), and digital images were taken with a microscope camera (Leica DFC700 T, Leica Microsystems) after the sections were examined.

Quantification of immunohistochemistry with ImageJ: For the purpose of evaluating and quantifying the fluorescence

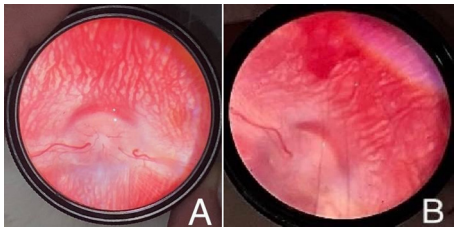

Figure 1. (A) Merangiotic structure of rabbit fundus and optic disc. (B) Vitreous hemorrhage observed immediately after application.

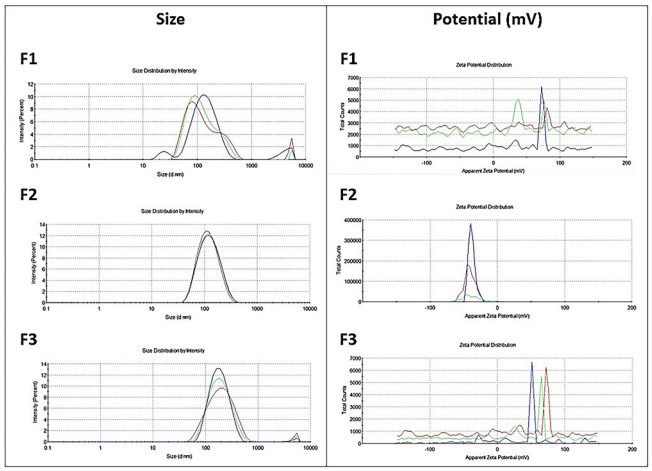

Figure 2. Size dimension and zeta potential of the nintedanib-liposome (NTB-LIP) formulations.

intensity with ImageJ (1.53j, 64 bit for Windows NIH), the digital images were taken at standard exposure. Area measurement was done after the program was calibrated using the "scale bar." The FITC channel of the images was then measured for intensity. The equation "Corrected fluorescence intensity measurement (CFIM) = Measured intensity – (measured area × average background measurement)" was used to calculate the corrected fluorescence intensity measurement.

Statistical analysis: Statistical analysis was executed using the SPSS program (version 22.0, SPSS Inc.). The Shapiro–Wilk test was used to evaluate the conformity of quantitative data with normal distribution. The Mann–Whitney U test was used for the data that did not show a normal distribution in comparisons of two independent groups. Fisher's exact test was used to compare qualitative data. Spearman correlation analysis was employed to gauge the extent of and correlation between two sets of quantitative data. Statistical significance was set at $p < 0.05$.

RESULTS

Determination of the optimal NTB-LIP formulation: The polydispersity index (PDI) parameter has an important role in particle size distribution, and its value should be less than 1 [15,34]. In our study, the PDI was found to be below 0.3 (0.15 ± 0.02) in F2 and statistically high in F1 (0.45 ± 0.11) and F3 (0.41 ± 0.09; $p < 0.05$; Figure 2). The electrical charge measured using the zeta mode gives clues about the stability of the liposomes. A ± 30–50 value means that the stability is good, and the negative value of F2 (−41.7 ± 0.2 mV) may positively affect the acceptability of the liposome against the positive load of the vitreous part [35,36]. Environmental factors such as pH and ionic strength are critical in influencing liposome stability. pH affects the ionization of lipids and the encapsulated drug, potentially destabilizing the liposomal membrane, while ionic strength can reduce electrostatic repulsion, leading to aggregation and compromising stability. Although zeta potential is a common in vitro measure of stability, it may not fully reflect in vivo conditions. The longevity of NTB in the vitreous is a more relevant indicator because it directly assesses how liposomes perform in physiologic environments, impacting their therapeutic efficacy [37,38].

SEM analysis was performed to confirm the DLS measurement results (Figure 3). It was determined that the diameter of the liposome structure in F2 was approximately 142.33 ± 2.58 nm, compared to 121.29 ± 9.55 nm in F1 and 138.06 ± 12.23 nm in F3. In the meantime, F2 liposomes exist in more homogeneous and uniform structures than the other formulations, which is consistent with the DLS results of the NTB-LIPs.

In terms of En. Ef. % comparison, the NTB amount of F2 (96.23% ± 1.28) was statistically different from those of F1 (85.29% ± 2.05) and F2 (77.3% ± 0.29; $p < 0.05$). F2, which underwent 10 freeze–thaw cycles, exhibited a higher En. Ef. % and an optimal PDI than F1 (three cycles) and F3 (five cycles). This suggests that the 10-cycle process is more effective in producing stable liposomes with desirable characteristics for drug delivery. Moreover, F2's HPLC peak was significantly lower toward the former version of the supernatant (before loading onto the liposome; Figure 4). Therefore, it was decided that the F2 formulation would be used as the optimal formulation in future studies.

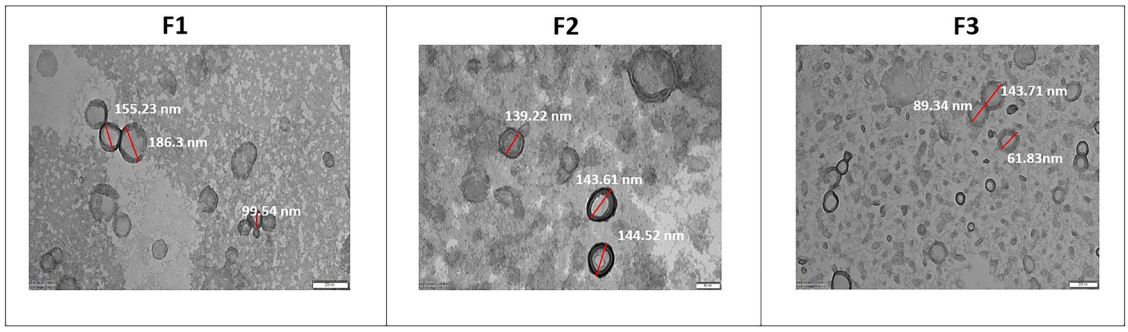

Figure 3. Microscope images of the NTB-LIP formulations.

ELISA, RT-PCR, and Western blot: There was a significant difference ($p < 0.05$) in mRNA expression levels between the NTB-LIP group and the control group (+), while no significant difference was observed in the other groups (markers). Similarly, the VEGF-A mRNA expression levels showed notable differences ($p < 0.01$). There was no statistically significant difference between the NTB-LIP and control groups. In contrast, there was a notable difference between the NTB-PBS and control groups (+) at both 12 and 24 h (differences of 30.6% and 29.2% for 12 and 24 h, respectively; $p < 0.01$). For TNF-α, the ratios between the NTB-PBS and control groups (+) were 25.6% and 25.4%, respectively, while for necrotic factor kappa beta (Nf-κβ), the variables were found to be 31.4% and 30.9% ($p < 0.001$). VEGF, TNF-α, and Nf-κβ are factors that induce apoptosis and cell destruction.

In contrast, in the Western blot protein analysis, the expression of TNF-α was decreased significantly ($p < 0.05$) with the administration of NTB-LIP and in the control group (+), and this decrease was alleviated with the administration of NTB-PBS. VEGF-A and Nf-κβ, which are vascular and mesenchymal markers, were significantly decreased (compared to the negative control group; $p < 0.001$). Our results proved that the cells treated with NTB-LIP further reversed this situation [39,40]. Furthermore, in Lauri et al.'s study, the cells treated using 5-fluorouracil (5-FU) loaded onto the liposome recovered much faster than the cells treated with normal 5-FU and with no difference from the control group [41].

Viability assay: After the cells were treated with the formulations at all concentrations, the variations between NTB-PBS and NTB-LIP were significant (21.7%, 30.2%, and 39.7% for 4.5 mM, 9 mM, and 18 mM, respectively). Furthermore, both NTB-PBS and NTB-LIP presented obvious variations in terms of each of these concentrations against the negative control group ($p < 0.001$; Figure 5). For NTB-LIP, the cell viability results were recorded as 97.4% ± 1.7%, 95.2% ± 1.1%, and 91.8% ± 2.0% for concentrations of 4.5 mM, 9.3 mM, and 18 mM, respectively ($p > 0.05$). The liposome formulations' concentrations showed no significant difference in the statistical analysis ($p > 0.05$; Figure 6).

Two separate factors are believed to account for the fact that liposome formulations have no deleterious influence on cell viability. This could likely stem from liposomes' protective function. This is crucial because the active substance is encapsulated into the liposome formulations. Therefore, the corrosion effect of the drug affects the cells [42]. In addition, IC_{50} was individually gauged for both NTB-LIP and NTB-PBS. The obtained IC_{50} values of NTB-PBS and NTB-LIP were 18.8 mM and 29.5 mM, respectively.

Scratch assay: In the NTB-LIP group, the scratch was not healed after 0 h (43.7% improvement), while this rate was 73.4% after 24 h (Figure 7; $p < 0.05$). In the NTB-PBS group,

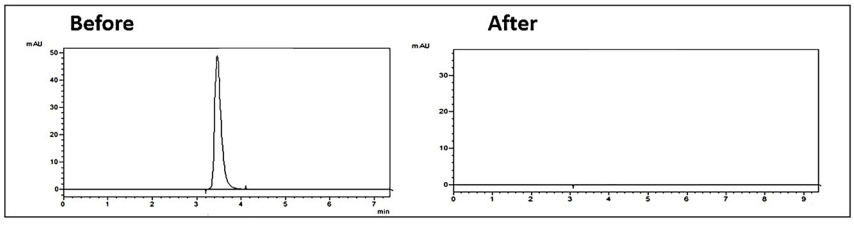

Figure 4. High-pressure liquid chromatograms before and after liposome addition.

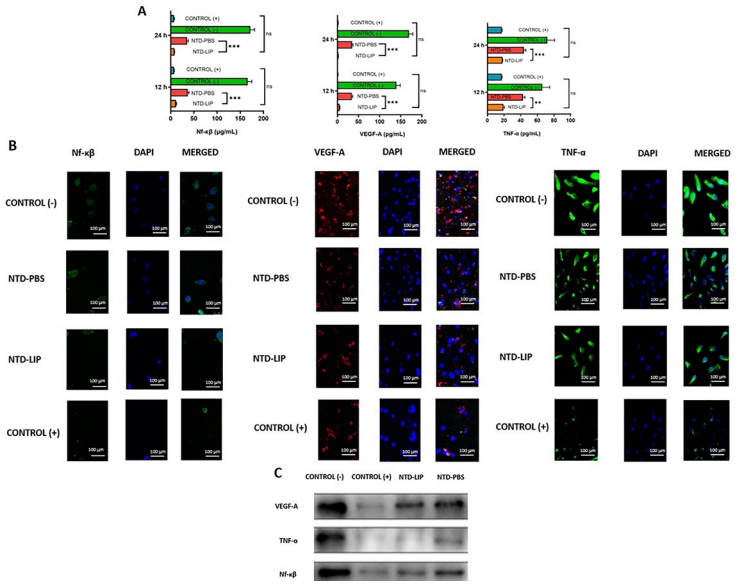

Figure 5. Expression levels of specific markers, whether treated with formulations or not. **A**: Formulations' marker levels. **B**: Fluorescence microscope image of the RPE cells after staining. **C**: Western blot protein dragging result (Nf-κβ: necrotic factor kappa beta; TNF-α: tumor necrosis factor alpha; VEGF-A: vascular endothelial growth factor A).

the incidence rates were 34.2% and 37.3%, respectively, after 0 and 24 h ($p > 0.05$). Ghasemi et al. proposed several targets for adjunctive therapies in PVR [43]. Therefore, the prevention of fibrin deposition, cellular migration and proliferation, antimetabolite agents, and tyrosine kinase inhibitors is effective in the recovery process of PVR [44]. Recent studies on the prophylactic treatment of PVR have focused on the inhibition of molecules involved in the PVR process, and the results of the present study support the findings of such studies.

Drug release results of the animal study: For NTB-LIP, the vitreous half-life was estimated to be 9.85 days, which was threefold greater than that of the NTB-PBS solution. In parallel, following a 0.5 mg/mL unilateral intravitreal injection of NTB-LIP in rabbit eyes (non-compartmental analysis), the concentrations remained above ~80 µg/mL for 37 days (Figure 8; Table 3). The minimal mobility of liposomes in vitreous humor, when effective, permits a large increase in the local half-life of active compounds [45]. To achieve excellent intravitreal pharmacokinetics, the size of the liposomes in the vitreous is of utmost importance. The elimination of NTB-LIP ($0.072h^{-1}$) in rabbits is thus ~3 times slower with the liposomal formulation than with LIP-PBS ($0.224\ h^{-1}$). In Nomoto et al.'s rabbit model study, longer vitreous half-lives of bevacizumab (BVC) liposomes (5.95 days) were discovered (unilateral injection), in contrast to the regular solution of BVC (3.23 days). The quantity of BVC in

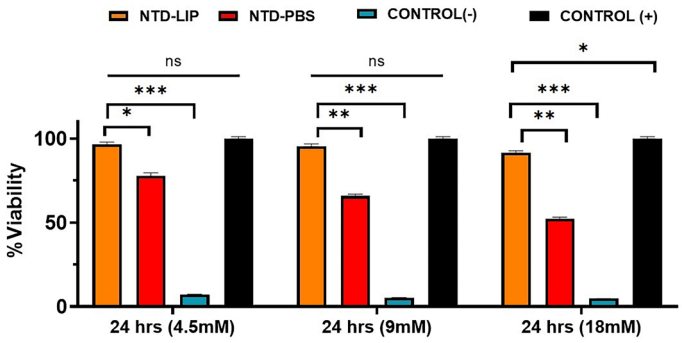

Figure 6. Viability assay to evaluate the formulations' toxicological formations.

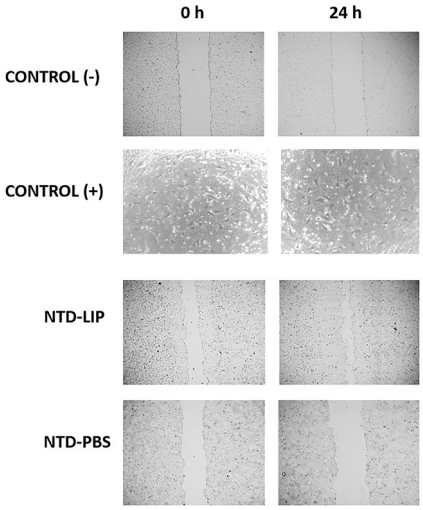

Figure 7. Migration study microscope images.

the iris/ciliary body and retina/choroids was also assessed, and half-lives of 5.74 and 6.23 days were obtained for these tissues, respectively [46].

Ophthalmologic examination: The stages of the control (C) and nintedanib (N) groups according to the Fastenberg classification are summarized in Table 4. In most of the subjects, signs of retinal detachment began to be observed within two to three weeks. Of the subjects treated with NTB, 66.7% (n = 4) were stage 1, 16.7% (n = 1) were stage 4, and 16.7% (n = 1) were stage 5. Of the subjects in the control group, 16.7% (n = 1) were stage 2, 33.3% (n = 2) were stage 4, and 50% (n = 3) were stage 5. According to the Fisher's exact test results, there was no statistically significant difference between the groups in terms of the subjects' clinical stages (: 6.333; p = 0.108). The fundus images of some subjects are shown in Figure 9.

In the anterior segment examination performed at week 4, inflammatory changes, such as lid edema, conjunctivitis, corneal edema, and reaction in the anterior chamber, were not observed in the 12 rabbits. Due to possible lens trauma, partial cataract formation, which would not interfere with

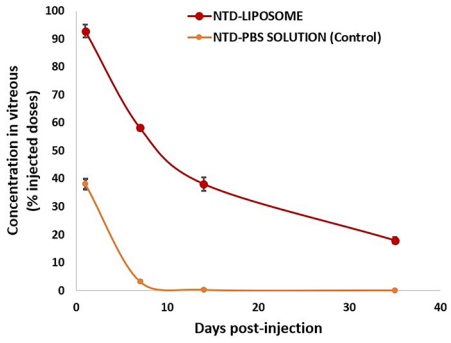

Figure 8. Dissolution profile of the NTB and NTB-LIP formulations.

Table 3. Pharmacokinetic parameters after collecting intravitreal sample from rabbits.

Formulation	Half-life (days)	MRT (days)	T_{max} (days)	Vitreous C_{max} (µg/ml)
NTB-LIP	9.85±0.53	39.2±0.7	1	412.9±2.5
NTB-PBS	3.21±0.23	8.3±0.5	1	196.8±1.4

MRT: Mean residency time, NTB-LIP: Nintedanib loaded liposome formulation, NTB-PBS: nintedanib solution in phosphate buffer saline, Tmax: Time to attain maximum concentration

Table 4. Fastenberg classification stages of the subjects according to the weeks.

Subject no.	1st week	2nd week	3rd week	4th week
C1	1	2	4	5
C2	1	2	2	2
C3	1	2	2	4
C4	1	3	3	4
C5	1	1	3	5
C6	1	4	4	5
N1	0	0	1	1
N2	1	1	2	1
N3	1	3	3	5
N4	0	1	1	1
N5	1	3	3	4
N6	0	1	1	1

C: Control group, N: Nintedanib group

fundus examination, was observed only in subjects N5 and C1. In cases where clinical evaluation could not be performed optimally due to media opacities such as cataract formation, excessive fibrosis, and total detachment, the enucleated eyes were dissected along the vertical meridian extending from the middle of the cornea to the optic disc, and the clinical stages were confirmed grossly through anatomic evaluation.

Histopathology and immunohistochemistry: In both the control and NTB groups, the cornea and sclera were observed along with all typical histological layers and cells. Vascular tissue was found between the iris and the lens in some rabbits in the control group, which was thought to be associated with the lens's subluxation. Only one rabbit in the experimental group had a similar histological structure, and the other rabbits did not show an increased vascular tissue feature in this area (Figure 10). Areas consistent with bleeding/thrombus were observed in the entry areas of the needle which used to create the disease model.

The choriocapillary layer was significantly thinner in the NTB group than in the control group when the posterior portion of the eye was examined. This difference between the groups was thought to be the result of the control group's edema being brought on by vein dilatation, whereas the experimental group may have experienced less edema as a result of the injection of NTB (Figure 11).

Fibrotic membrane formations were seen in front of the retina and ciliary body in the control tissue, which was

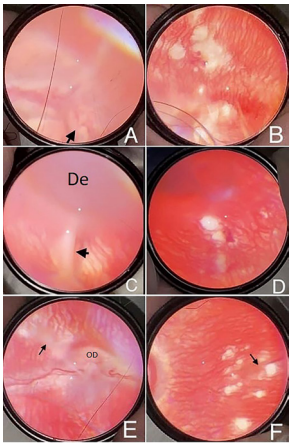

Figure 9. Fundus images of the rabbits. **A**: Total retinal detachment; the optic disc is indicated by an arrow (↑;subject no. C1, stage 5). **B**: Focal traction and intravitreal membrane formations and gliotic changes in the retina (subject no. C2, stage 2). **C**: Traction creating a membrane (↑) and a wide detachment area (De; subject no. C4, stage 4). **D**: Intravitreal membrane, vitreous opacities, and gliotic changes in the retina (subject no. N1, stage 1). **E**: Membrane extending from the disc (OD) and that does not produce traction, indicated by an arrow (↑;subject no. N2, stage 1). (F) Intravitreal membrane indicated by an arrow (↑), and gliotic changes in the retina (subject no. N6, stage 1).

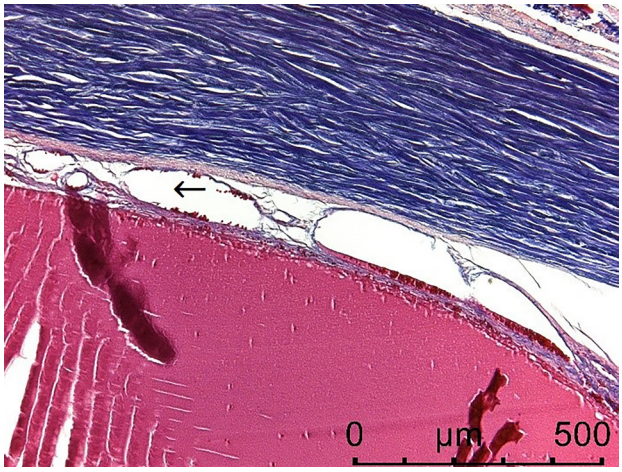

Figure 10. Vascular tissue (←) attached to the lens (100×).

consistent with the epiretinal membrane anticipated to be seen in the disease model. In the group receiving NTB, it was discovered that the fibrotic membranes were lessened in front of the retina and absent in front of the iris (Figure 12).

Two of the subjects in the NTB group showed changes in the iris that resembled papillary structures, which were thought to have been caused by the drug, as well as corrugation in the retina and an opaque region around the iris in one of the animals (Figure 13).

The CFIM results of the subjects for collagen-1 in the control group and those in the NTB-treated group are shown in Figure 14. According to the Mann–Whitney U test results, the CFIM level of the NTB group was significantly lower than that of the control group ($p = 0.004$). In Spearman correlation analysis, a positive and highly statistically significant correlation between clinical stage and CFIM was found in the control group ($r = 0.926$; $p = 0.008$). However, in the NTB group, no correlation between stage and CFIM was found ($r = 0.135$; $p = 0.798$).

DISCUSSION

The etiology of surgical failure in rhegmatogenous retinal detachment, or PVR, remains largely unknown. However, many growth factors and cytokines are considered to be the main players [7]. Although surgery is currently the standard treatment for PVR, the identification of inflammatory mediators provides new and effective therapeutic targets for the treatment of PVR [47]. Many anti-inflammatory, antiproliferative, antineoplastic, growth inhibitory, and antioxidant agents for these targets have been tested in both preclinical and clinical studies for the treatment and prophylaxis of PVR. However, there is currently no pharmacological agent that has been proven to be effective in the treatment and prevention of PVR [4].

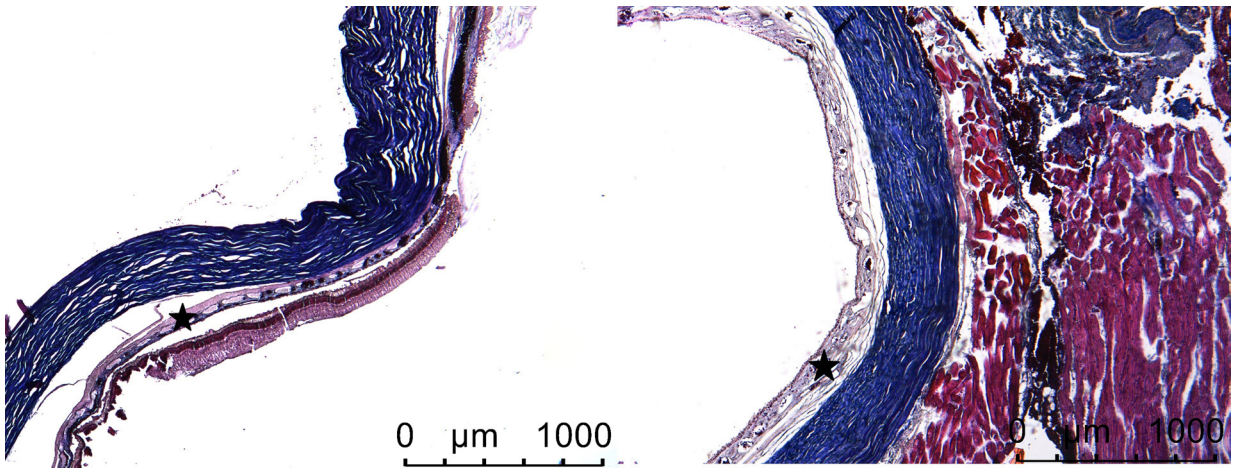

Figure 11. A choriocapillary layer (star) thinner in the NTB group (left) than in the control group (right; 40×).

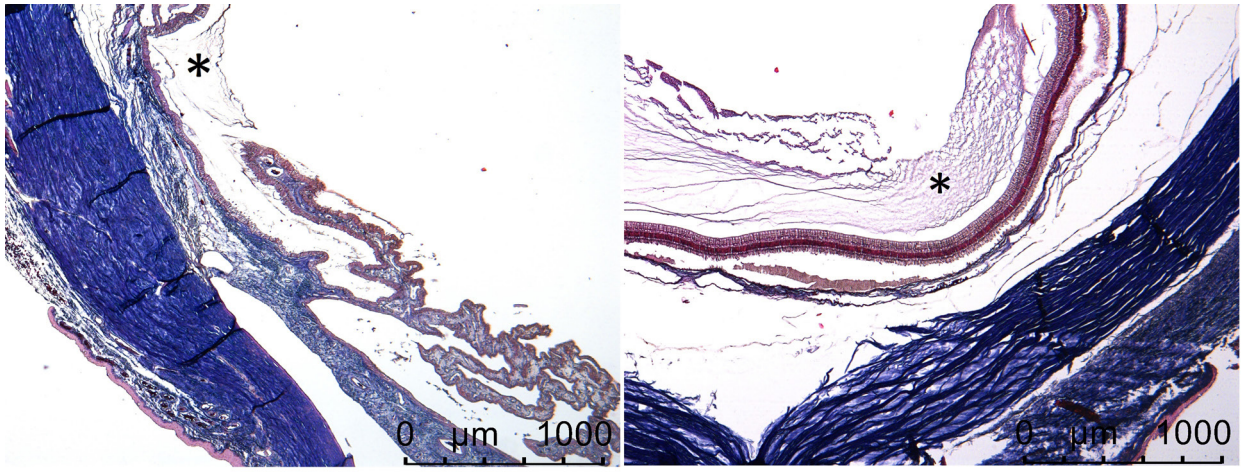

Figure 12. Fibrotic membrane formations in the NTB (left) and control (right) groups. The asterisk indicates fibrotic membranes (40×).

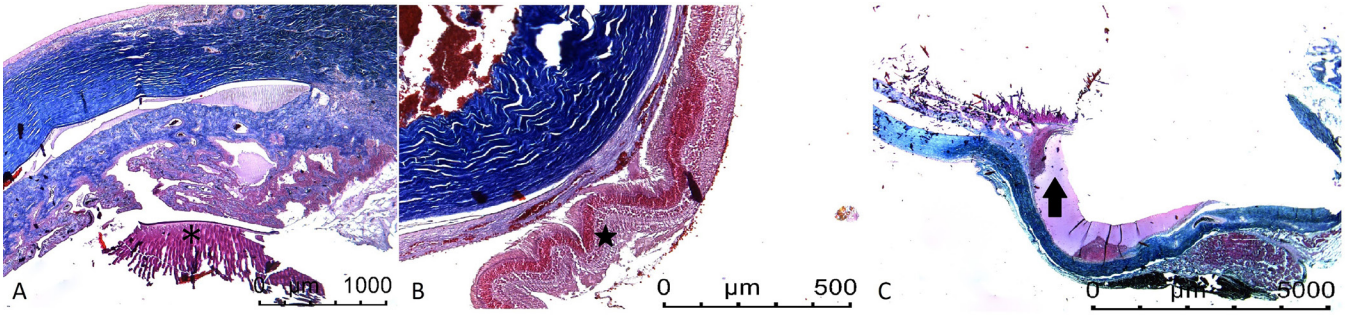

Figure 13. Histology sections of the subjects in the NTB group. **A**: Papillary changes (*; 40×). **B**: Corrugation in the retina (star; 100×). **C**: Opaque region (↑; 12.5×).

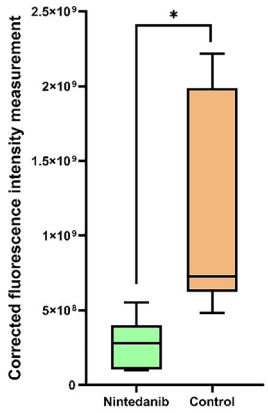

Figure 14. Corrected fluorescence intensity measurement (CFIM) results of the NTB and control groups. Statistical analysis (Mann–Whitney U test) indicated that the CFIM level of the NTB group was significantly lower than that of the control group (p = 0.004).

Several methods have been described in the literature to induce the experimental PVR model in animals. Among these are artificial trauma, intravitreal cell injection, intravitreal injection of cytokine or growth factor, surgical manipulations (vitrectomy, retinotomy, cryopexy, gas compression), injection of dispase, and injection of platelet-rich plasma (PRP) or blood [48]. Considering the advantages and disadvantages of all these methods, the minimal dispase injection model [32], which was shown to be effective, combined with artificial trauma, was used in our study to mimic an appropriate experimental PVR model. Furthermore, the progression of PVR in animal models is generally much faster than in humans, although there is a variable time period for different models. Retinal detachment can occur within days, and most models progress to full PVR development by four weeks [48]. In our study, signs of detachment began to appear within two to three weeks, and the experiment was completed in four weeks.

Liposomes are vesicular nanocarrier systems consisting of one or more compartments prepared with phospholipids. These formulations act as “reservoir-type” carriers and are therefore considered among the carrier systems that are ideal for use in the posterior segment of the eye [11]. The advantages of liposomal delivery of drugs are reduced dosing frequency, reduced peak concentrations resulting in reduced toxicity, a higher therapeutic index, and the ability to passively target the mononuclear phagocytic system. Liposomes are particularly effective for the treatment of diseases affecting the phagocytes of the immune system because they accumulate in phagocytes, which recognize them as foreign invaders. For this reason, the use of liposome-encapsulated drugs to treat PVR was first recognized after previous studies showed that RPE cells are phagocytic and that liposomes are phagocytosed by cells of the reticuloendothelial system [49,50]. Our study aimed to explore the potential of delivering sustained-release formulations to the eye using injection into the vitreal space, particularly using negatively charged liposomes, considering the pathogenesis of the disease. Specifically, we focused on entrapping NTB to better control its release for intravitreal administration. Our findings showed a high NTB entrapment efficiency of approximately 70% using PhoCH liposomes. Furthermore, we observed slower transport and in vivo release for the 37-day studies, with a significant difference in transport ($p = 0.009$; $p < 0.05$) based on the Mann–Whitney U test results. The differences in transport for the various liposomes studied are attributed to their depth of penetration in the vitreous and the differences in their release kinetics.

Recently, there have been various ophthalmological studies, both in vivo and in vitro, on NTB, which has been approved for IPF treatment. Rivera et al. conducted a study on rats to test the effectiveness of NTB on vaso-obliteration (VO) and preretinal neovascularization (NV) models. The VO model did not indicate any increase in VO with NTB, but the NV model showed that NTB sped up the process of normal retinal vascularization and decreased preretinal NV compared to the vehicle. They suggested that NTB could be an alternative to anti-VEGF therapies for the treatment of ischemic retinopathies [51]. Khanum et al. demonstrated via clinical evaluation, histopathology, and immunohistochemistry that intravitreally administered pirfenidone, another drug approved by the FDA for IPF, prevents PVR formation in a post-traumatic PVR model in rabbits [30]. Deissler et al. found that NTB completely reversed the VEGF-A165-induced barrier dysfunctions formed by retinal endothelial cells or long-term cultivated ARPE-19 cells [52]. Yin et al. showed that NTB inhibits the epithelial-mesenchymal transition; the development of the disease is heavily influenced by PVR and induced with TGF-β2 in retinal pigment epithelial cells. Therefore, they proposed a potential pharmacological treatment for PVR [53].

Based on our research, it is evident that the NTB group had significantly lower levels of collagen-1, as measured through CFIM, than the control group ($p = 0.004$). This is a crucial finding. There was no significant difference between the clinical stages of the NTB and control groups ($p = 0.108$). The outcome may have been influenced by the insufficient number of participants in each group. However, it is worth noting that the NTB group exhibited reduced fibrotic membrane formation in front of the retina during histological examination, consistent with the results of the immunofluorescence measurements. A positive and highly statistically significant correlation between clinical stage and CFIM was found in the control group ($r = 0.926$; $p = 0.008$), but no correlation between the two variables was found in the NTB group ($r = 0.135$; $p = 0.798$). While there was a significant difference between the Fastenberg stage and CFIM for collagen-1 in the control group, there was none in the NTB group, perhaps due to the disruption of the usual PVR process by intravitreal NTB administration.

Conclusion: Our study has provided preclinical support for a liposomal formulation containing NTB that has the potential to be effective in vivo in preventing the development of PVR and its correlated pathologies. This drug has achieved the desired outcomes without causing any major side effects. Liposomal encapsulation ensured a prolonged effect with a single-dose application, thereby reducing the need for

multiple repetitive applications. Our study has conclusively demonstrated the efficacy of NTB in reducing PVR in an animal model, paving the way for more efficient and effective solutions that can replace invasive intravitreal injections. Further research exploring the effects of varying concentrations and different models with experiments involving more animals is necessary to fully realize the potential of this technology in preventing and potentially treating PVR.

ACKNOWLEDGMENTS

The authors express their gratitude to Hacettepe University's Scientific Research Projects Coordination Unit for the funding, and to the Department of Histology and Embryology at Hacettepe University and the Department of Pharmaceutical Technology at Yeditepe University for providing the necessary facilities. Contributions of the Author EA, FO, BU: methodology, validation, data curation, formal analysis. BU, CT, ST, SFM: imaging and instrumentation; EA, FO: animal study and data interpretation, EA, FO, BU, ST, SFM, CT: conceptualization, methodology, writing – review and editing, supervision, formal analysis. Ethical Approval The study has been granted approval by both the Hacettepe University Animal Experiments Local Ethics Committee (Approval No. 2020/54) and the Yeditepe University Animal Experiments Local Ethics Committee (Approval No. 2021–868). All methods were performed in accordance with the relevant guidelines and regulations. Competing interests The authors unequivocally declare that they possess no conflicts of interest. Furthermore, they assert that they have meticulously scrutinized and granted their endorsement to the published version of the manuscript. Fundings or Grants This work was supported by the Scientific Research Projects Coordination Unit of Hacettepe University under grant (number THD202119176). Availability of data and materials There is no data set available

REFERENCES

1. Hilton G, Machemer R, Michels R, Okun E, Schepens C, Schwartz A. The classification of retinal detachment with proliferative vitreoretinopathy. Ophthalmology 1983; 90:121-5. [PMID: 6856248].
2. Ryan SJ. The pathophysiology of proliferative vitreoretinopathy in its management. Am J Ophthalmol 1985; 100:188-93. [PMID: 4014372].
3. Pastor JC. Proliferative vitreoretinopathy: an overview. Surv Ophthalmol 1998; 43:3-18. [PMID: 9716190].
4. Idrees S, Sridhar J, Kuriyan AE. Proliferative vitreoretinopathy: A review. Int Ophthalmol Clin 2019; 59:221-40. [PMID: 30585928].
5. Pastor JC, de la Rúa ER, Martín F. Proliferative vitreoretinopathy: risk factors and pathobiology. Prog Retin Eye Res 2002; 21:127-44. [PMID: 11906814].
6. Wu F, Eliott D. Molecular Targets for Proliferative Vitreoretinopathy. Semin Ophthalmol 2021; 36:218-23. [PMID: 33616467].
7. Sadaka A, Giuliari GP. Proliferative vitreoretinopathy: current and emerging treatments. Clin Ophthalmol 2012; 6:1325-33. [PMID: 22942638].
8. Shahlaee A, Woeller CF, Philp NJ, Kuriyan AE. Translational and clinical advancements in management of proliferative vitreoretinopathy. Curr Opin Ophthalmol 2022; 33:219-27. [PMID: 35220328].
9. Ofev FL. (Nintedanib): First Tyrosine Kinase Inhibitor Approved for the Treatment of Patients with Idiopathic Pulmonary Fibrosis. Am Health Drug Benefits 2015; 8:101-4. .
10. Wind S, Schmid U, Freiwald M, Marzin K, Lotz R, Ebner T, Stopfer P, Dallinger C. Clinical Pharmacokinetics and Pharmacodynamics of Nintedanib. Clin Pharmacokinet 2019; 58:1131-47. [PMID: 31016670].
11. Guidetti B, Azéma J, Malet-Martino M, Martino R. Delivery systems for the treatment of proliferative vitreoretinopathy: materials, devices and colloidal carriers. Curr Drug Deliv 2008; 5:7-19. [PMID: 18220546].
12. Amoabediny G, Haghiralsadat F, Naderinezhad S. Overview of preparation methods of polymeric and lipid-based (niosome, solid lipid, liposome) nanoparticles: A comprehensive review. Int J Polym Mater 2018; 67:383-400. .
13. Teixeira MC, Carbone C, Souto EB. Beyond liposomes: Recent advances on lipid based nanostructures for poorly soluble/poorly permeable drug delivery. Prog Lipid Res 2017; 68:1-11. [PMID: 28778472].
14. Costa AP, Xu X, Burgess DJ. Freeze-anneal-thaw cycling of unilamellar liposomes: effect on encapsulation efficiency. Pharm Res 2014; 31:97-103. [PMID: 23881305].
15. Üner B, Özdemir S, Taş Ç, Özsoy Y, Üner M. Development of lipid nanoparticles for transdermal loteprednol etabonate delivery. J Microencapsul 2022; 39:327-40. [PMID: 35583383].
16. Purnachand D, Veerareddy A, Ramadevi B, Kameswarrao ChV, Madhusudhanreddy B. Development and Validation of a RP-HPLC Method for Determination of Related Substances and Degradants in Entacapone. J Chromatogr Sci 2016; 54:1310-23. [PMID: 27165569].
17. Xiao Y, Choi KS, Warther D, Huffman K, Landeros S, Freeman WR, Sailor MJ, Cheng L. A sustained dual drug delivery system for proliferative vitreoretinopathy. Drug Deliv 2020; 27:1461-73. [PMID: 33100053].
18. Ali RO, Quinn GM, Umarova R, Haddad JA, Zhang GY, Townsend EC, Scheuing L, Hill KL, Gewirtz M, Rampertaap S, Rosenzweig SD, Remaley AT, Han JM, Periwal V, Cai H, Walter PJ, Koh C, Levy EB, Kleiner DE, Etzion O, Heller T. Longitudinal multi-omics analyses of the gut-liver axis

reveals metabolic dysregulation in hepatitis C infection and cirrhosis. Nat Microbiol 2023; 8:12-27. [PMID: 36522461].

19. Fattore L, Cafaro G, Di Martile M, Campani V, Sacconi A, Liguoro D, Marra E, Bruschini S, Stoppoloni D, Cirombella R, De Nicola F, Pallocca M, Ruggiero CF, Castaldo V, Catizone A, Del Bufalo D, Viglietto G, Vecchione A, Blandino G, Aurisicchio L, Fanciulli M, Ascierto PA, De Rosa G, Mancini R, Ciliberto G. Oncosuppressive miRNAs loaded in lipid nanoparticles potentiate targeted therapies in BRAF-mutant melanoma by inhibiting core escape pathways of resistance. Oncogene 2023; 42:293-307. [PMID: 36418472].

20. Fujimori T, Shibayama Y, Kanda T, Suzuki K, Ogawa D, Ishikawa R, Kadota K, Matsunaga T, Tamiya T, Nishiyama A, Miyake K. Effects of a monoclonal antibody against (pro) renin receptor on gliomagenesis. Sci Rep 2023; 13:808- [PMID: 36646875].

21. Santos Lacomba M, Marcos Martín C, Gallardo Galera JM, Gómez Vidal MA, Collantes Estévez E, Ramírez Chamond R, Omar M. Aqueous humor and serum tumor necrosis factor-α in clinical uveitis. Ophthalmic Res 2001; 33:251-5. [PMID: 11586057].

22. Mudawadkar AD, Sonawane GH, Patil TJ. Thermodynamics of micellization of nonionic surfactant Triton X-100 in presence of additive Poly-N-Vinyl-Pyrrolidone using clouding phenomenon. Orient J Chem 2013; 29:227-33. .

23. Pastor JC, Rojas J, Pastor-Idoate S, Di Lauro S, Gonzalez-Buendia L, Delgado-Tirado S. Proliferative vitreoretinopathy: A new concept of disease pathogenesis and practical consequences. Prog Retin Eye Res 2016; 51:125-55. [PMID: 26209346].

24. Wang M, Li Q, Dong H. Proteomic evidence that ABCA4 is vital for traumatic proliferative vitreoretinopathy formation and development. Exp Eye Res 2019; 181:232-9. [PMID: 30738069].

25. Hafezi Moghaddam R, Dadfarnia S, Shabani AMH, Moghaddam ZH, Tavakol M. Electron beam irradiation synthesis of porous and non-porous pectin based hydrogels for a tetracycline drug delivery system. Mater Sci Eng C Mater Biol Appl 2019; 102:391-404. [PMID: 31147010].

26. Murali K, Kenesei K, Li Y, Demeter K, Környei Z, Madarász E. Uptake and bio-reactivity of polystyrene nanoparticles is affected by surface modifications, ageing and LPS adsorption: in vitro studies on neural tissue cells. Nanoscale 2015; 7:4199-210. [PMID: 25673096].

27. Cevik O, Acidereli H, Turut FA, Yildirim S, Acilan C. Cabazitaxel exhibits more favorable molecular changes compared to other taxanes in androgen-independent prostate cancer cells. J Biochem Mol Toxicol 2020; 34:e22542[PMID: 32578930].

28. Klettner A, Tahmaz N, Dithmer M, Richert E, Roider J. Effects of aflibercept on primary RPE cells: toxicity, wound healing, uptake and phagocytosis. Br J Ophthalmol 2014; 98:1448-52. [PMID: 25034050].

29. Zhang Y, Huo M, Zhou J, Zou A, Li W, Yao C, Xie S. DDSolver: an add-in program for modeling and comparison of drug dissolution profiles. AAPS J 2010; 12:263-71. [PMID: 20373062].

30. Khanum BNMK, Guha R, Sur VP, Nandi S, Basak SK, Konar A, Hazra S. Pirfenidone inhibits post-traumatic proliferative vitreoretinopathy. Eye (Lond) 2017; 31:1317-28. [PMID: 28304388].

31. Frenzel EM, Neely KA, Walsh AW, Cameron JD, Gregerson DS. A new model of proliferative vitreoretinopathy. Invest Ophthalmol Vis Sci 1998; 39:2157-64. [PMID: 9761295].

32. Kralinger MT, Kieselbach GF, Voigt M, Hayden B, Hernandez E, Fernandez V, Parel JM. Experimental model for proliferative vitreoretinopathy by intravitreal dispase: limited by zonulolysis and cataract. Ophthalmologica 2006; 220:211-6. [PMID: 16785750].

33. Fastenberg DM, Diddie KR, Dorey K, Ryan SJ. The role of cellular proliferation in an experimental model of massive periretinal proliferation. Am J Ophthalmol 1982; 93:565-72. [PMID: 7081355].

34. Gönüllü Ü, Üner M, Yener G, Karaman EF, Aydoğmuş Z. Formulation and characterization of solid lipid nanoparticles, nanostructured lipid carriers and nanoemulsion of lornoxicam for transdermal delivery. Acta Pharm 2015; 65:1-13. [PMID: 25781700].

35. Souto EB, Wissing SA, Barbosa CM, Müller RH. Development of a controlled release formulation based on SLN and NLC for topical clotrimazole delivery. Int J Pharm 2004; 278:71-7. [PMID: 15158950].

36. Müller RH, Shegokar R, Keck CM. 20 years of lipid nanoparticles (SLN and NLC): present state of development and industrial applications. Curr Drug Discov Technol 2011; 8:207-27. [PMID: 21291409].

37. Pasarin D, Ghizdareanu AI, Enascuta CE, Matei CB, Bilbie C, Paraschiv-Palada L, Veres PA. Coating Materials to Increase the Stability of Liposomes. Polymers (Basel) 2023; 15:782- [PMID: 36772080].

38. Makino K, Yamada T, Kimura M, Oka T, Ohshima H, Kondo T. Temperature- and ionic strength-induced conformational changes in the lipid head group region of liposomes as suggested by zeta potential data. Biophys Chem 1991; 41:175-83. [PMID: 1773010].

39. Crisostomo PR, Wang M, Herring CM, Markel TA, Meldrum KK, Lillemoe KD, Meldrum DR. Gender differences in injury induced mesenchymal stem cell apoptosis and VEGF, TNF, IL-6 expression: role of the 55 kDa TNF receptor (TNFR1). J Mol Cell Cardiol 2007; 42:142-9. [PMID: 17070836].

40. Beierle EA, Strande LF, Chen MK. VEGF upregulates BCL-2 expression and is associated with decreased apoptosis in neuroblastoma cells. In: *Journal of Pediatric Surgery.* Vol 37. W.B. Saunders; 2002:467–471.

41. Luput L, Sesarman A, Porfire A, Achim M, Muntean D, Casian T, Patras L, Rauca VF, Drotar DM, Stejerean I, Tomuta I, Vlase L, Dragos N, Toma VA, Licarete E, Banciu M. Liposomal simvastatin sensitizes C26 murine colon carcinoma

to the antitumor effects of liposomal 5-fluorouracil in vivo. Cancer Sci 2020; 111:1344-56. [PMID: 31960547].

42. Rahamathulla M, H v G, Veerapu G, Hani U, Alhamhoom Y, Alqahtani A, Moin A. Characterization, Optimization, In Vitro and In Vivo Evaluation of Simvastatin Proliposomes, as a Drug Delivery. AAPS PharmSciTech 2020; 21:129- [PMID: 32405982].

43. Ghasemi Falavarjani K. Proliferative vitreoretinopathy and genetic profile. J Ophthalmic Vis Res 2013; 8:92-3. [PMID: 23825722].

44. Nassar K, Lüke J, Lüke M, Kamal M, Abd El-Nabi E, Soliman M, Rohrbach M, Grisanti S. The novel use of decorin in prevention of the development of proliferative vitreoretinopathy (PVR). Graefes Arch Clin Exp Ophthalmol 2011; 249:1649-60. [PMID: 21735240].

45. Mohammadi ZA, Aghamiri SF, Zarrabi A, Talaie MR. Liposomal Doxorubicin Delivery Systems: Effects of Formulation and Processing Parameters on Drug Loading and Release Behavior. Curr Drug Deliv 2016; 13:1065-70. [PMID: 26708673].

46. Nomoto H, Shiraga F, Kuno N, Kimura E, Fujii S, Shinomiya K, Nugent AK, Hirooka K, Baba T. Pharmacokinetics of bevacizumab after topical, subconjunctival, and intravitreal administration in rabbits. Invest Ophthalmol Vis Sci 2009; 50:4807-13. [PMID: 19324856].

47. Dai Y, Dai C, Sun T. Inflammatory mediators of proliferative vitreoretinopathy: hypothesis and review. Int Ophthalmol 2020; 40:1587-601. [PMID: 32103371].

48. Hou H, Nudleman E, Weinreb RN. Animal Models of Proliferative Vitreoretinopathy and Their Use in Pharmaceutical Investigations. Ophthalmic Res 2018; 60:195-204. [PMID: 29723860].

49. Patel HM. Serum opsonins and liposomes: their interaction and opsonophagocytosis. Crit Rev Ther Drug Carrier Syst 1992; 9:39-90. [PMID: 1544174].

50. Ebrahim S, Peyman GA, Lee PJ. Applications of liposomes in ophthalmology. Surv Ophthalmol 2005; 50:167-82. [PMID: 15749307].

51. Rivera JC, Noueihed B, Omri S, Barrueco J, Hilberg F, Chemtob S. BIBF1120 (Vargatef) Inhibits Preretinal Neovascularization and Enhances Normal Vascularization in a Model of Vasoproliferative Retinopathy. Invest Ophthalmol Vis Sci 2015; 56:7897-907. [PMID: 26670826].

52. Deissler HL, Stutzer JN, Lang GK, Grisanti S, Lang GE, Ranjbar M. VEGF receptor 2 inhibitor nintedanib completely reverts VEGF-A165-induced disturbances of barriers formed by retinal endothelial cells or long-term cultivated ARPE-19 cells. Exp Eye Res 2020; 194:108004.

53. Yin Y, Liu S, Pu L, Luo J, Liu H, Wu W. Nintedanib prevents TGF-β2-induced epithelial-mesenchymal transition in retinal pigment epithelial cells. Biomed Pharmacother 2023; 161:114543[PMID: 36933383].